



OPEN Impact of Navier's slip and MHD on laminar boundary layer flow with heat transfer for non-Newtonian nanofluid over a porous media

T. Maranna¹, S. M. Sachhin¹, U. S. Mahabaleshwar^{1✉} & M. Hatami^{2✉}

The current studies analytically summarize the impact of magnetohydrodynamic and thermal radiation on the non-Newtonian continuous uniform motion of viscid non-compressible nanofluid across a penetrable stretching/shrinking sheet, even though accomplish Navier's first and second order slips along mass transpiration. Blood-bearing silver and copper nanomaterials have distinct flow and heat transfer properties when exposed to heat. Silver (Ag) as well as copper (Cu) nanoparticles are assumed to be present in blood as the non-Newtonian liquid; this fluid serves as the base. We anticipate that the current study will be useful in fields including food, petrochemical products, and medicines, as well as blood circulation, and highly beneficial for patients who are dealing with blood clotting in the uterus, which may result in infertility or cancer, to evaluate the blood flow in the tube. Employing the similarity conversion technique, the ruling partial differential equations are modified into a couple of non-linear ordinary differential equations. Then the transformed ordinary differential equations are analytically solved with the Laplace transformation and expressed in terms of an incomplete gamma function. The current analytical results are compared to previous studies. It is addressed how several physical features such as magnetic field M , Navier's first and second order slip, permeability, Prandtl number Pr , and radiation parameter affect non-dimensional velocity as well as temperature patterns through graphs. The results obtained reveal that there is an enhancement in the rate of heat transfer with the rise in nanoparticle volume fraction and radiation. The temperature distribution is also influenced by the presence of Prandtl numbers, radiation, solid volume fraction, permeability, and slip conditions. This shows that the solid volume fraction of nanoparticles can be used to control the behaviour of heat transfer and nanofluid flows.

Abbreviations

A	Constant (-)
B	Constant (-)
B_0	Magnetic field (Tesla)
c	Constant (-)
C_p	Specific heat ($\text{JK}^{-1} \text{kg}^{-1}$)
d	Stretching/shrinking parameter (-)
f	Velocity similarity function (-)
K	Permeability (N/A^2)
K_1	Inverse Darcy number (-)
k^*	Mean absorption coefficient (cm^{-1})
M	Hartmann factor (-)
m, n	Constants (-)
N_r	Radiation parameter (-)

¹Department of Studies in Mathematics, Shivagangotri, Davangere University, Davangere, India. ²Department of Mechanical Engineering, Esfarayen University of Technology, Esfarayen, North Khorasan, Iran. ✉email: u.s.m@davangereuniversity.ac.in; m-hatami@um.ac.ir

Pr	Prandtl number (–)
q	Function of (u, v) (–)
q_t	Rate of change of q with respect to time (–)
q_r	Radiative heat flux (Wm^{-2})
T	Fluid temperature (K)
T_w	Temperature of surface (K)
T_∞	Ambient temperature (K)
u, v	X and y axes velocity coefficients ($m\ s^{-1}$)
V_c	Mass suction/injection factor (–)
x, y	Horizontal and vertical axis (–)
$(\rho C_p)_{nf}$	Heat capacitance of nanofluid ($JK^{-1}\ kg^{-1}$)
$(\rho C_p)_f$	Heat capacitance of fluid ($JK^{-1}\ kg^{-1}$)

Greek symbols

λ_1	First order slip (–)
λ_2	Second order slip (–)
α	Constant (–)
$\Gamma_1, \Gamma_2, \Gamma_3, \Gamma_4$	Coefficients (–)
ξ	Temperature jump constant (–)
ξ_1, ξ_2	Slip conditions (–)
κ_{nf}	Thermal conductivity of nanofluid (Wm^{-1}/K)
μ_{nf}	Dynamic viscosity of the nanofluid ($Ns\ m^{-2}$)
μ_f	Dynamic viscosity of the fluid ($Ns\ m^{-2}$)
η	Similarity variable (–)
θ	Temperature similarity variable (–)
ν_{nf}	Kinematic viscosity of the nanofluid ($m^2\ s^{-1}$)
ν_f	Kinematic viscosity of the fluid ($m^2\ s^{-1}$)
ρ_{nf}	Density of the nanofluid ($kg\ m^{-3}$)
ρ_f	Fluid density ($kg\ m^{-3}$)
σ_{nf}	Electrical conductivity of nanofluid (S/m)
σ^*	Stefan–Boltzmann constant (–)
ϕ	Solid volume fraction (–)
χ	Thermal diffusivity ($m^2\ s^{-1}$)

Abbreviations

nf	Nanofluid (–)
ODEs	Ordinary differential equations (–)
PDEs	Partial differential equations (–)
MHD	Magnetohydrodynamics (–)

For the past 20 years, various applications that are presently in use or that are intended have stimulated intensive research towards nanofluids or suspensions with nanoparticles. Although nanoparticles are employed in the flow regime throughout all real-world scenarios, the structure of the flow is dictated by the appropriate thermophysical properties of these nanofluids. Recently, nanofluids have been implemented for industrial and technological purposes. Printing, photovoltaic panels, geothermal power systems, electronic items, nanoscale gadgets for illness, refrigeration of metallic particles, microprocessors, lasers, cardboard boxes, and inkjets are only a few possibilities for nanoparticles. 100-nm-diameter nanocomposites are a mixture of solid and liquid nanostructures. The concept of nanofluids is described by Choi et al.¹ as being initially used in order to optimize the materials thermal performance. Eastman et al.² developed Copper nanoparticles were immersed in a polyethylene glycol-based nanoliquid that had greater heat stability than almost any other conventional base liquid, particularly ethylene glycol.

Usually, the nanomaterials used within nanoliquids consist of metals (aluminium, copper), oxides (aluminium oxides), nitrides (aluminium nitrate, silicon nitrate), carbides (silicon carbide), or non-metals (CNTs, graphite). Additionally, biological research seems to be employing a variety of fragments, including deoxyribonucleic acid, ribonucleic acid, biomolecules, and fluids articulated in porous materials^{3–5}. Researchers focusing on global ecosystems have recently raised thermal conductivity and optimized heat transportation characteristics by mixing two or more nanoparticles into a common base liquid. In works like those by researchers^{6–13}, initiatives to address the mobility of nanoparticles under several circumstances as well as their features are shown. The study of connections among electromagnetic forces as well as electrically conducting fluids is described as magnetohydrodynamics. The Swedish researcher Hannes Alves et al.¹⁴ developed the concept of MHD. Nowadays, magnetic fields are extensively employed in numerous major industries. In refrigeration or heating techniques, the magnetic situation is taken into account to enhance thermal performance. Because of its broad range of implications, the researchers used the magnetic field effect.

The latest study by Mahabaleshwar et al.^{15–20} on the casson hybrid nanofluid, nanofluids, dusty fluids, and carbon nanotubes physical phenomena under the presence of MHD and heat transfer along mass transpiration due to stretching/shrinking surfaces is discussed. Due to its special features, silver has a broad range of biological

purposes. Generally, silver-containing products are employed to fight a wide range of bacteria. Additionally, according to verifiable studies, Ag nanoparticles can replace conventional anticancer treatments in a manner that is more ecologically responsible and biodegradable²¹. The most significant biological fluid is blood, which is a fluid made up of many types of cells dispersed in a soluble fluid medium (the plasma). It ought to be emphasized that red blood cells in plasma have a role in rotational motion whenever a relative velocity arises. The body's cells have both an angular orbital momentum and an angular gyration moment. Hence, blood can be conceived as a non-Newtonian fluid with a uniform density. There are a variety of polar fluid hypotheses that can be explored, notably Stokes concept²².

Researchers and scientists from all around the universe have been working on various features of nanotechnology over the past few decades. For a bio-nanofluid, Ghassemi et al.²³ studied a new efficient thermal conductance concept (blood with nanoparticle Al₂O₃). A good deal of researchers^{24,25} are investigating theoretical studies that address the non-Newtonian blood circulation in stenotic arteries because capillary membranes are perhaps stretchy, absorptive, and changeable. Moreover, human blood was used as a base fluid to investigate heat convective boundary movements^{26,27}. To date, the trustworthy literature regarding recent developments in this fluid flow can be found in Refs.^{28–33}.

To the author's best knowledge and inspired by the aforementioned studies and potential implications in the current work, it is important to examine the impacts of magnetohydrodynamics as well as heat radiation on the Navier's first and second order slips along mass transpiration in a non-Newtonian constant laminar stream of viscous incompressible nanofluid across a porous stretching/shrinking surface. By using a similarity conversation, the associated partial differential equations for dominating flow are converted via a system of ordinary differential equations. Analytical approaches are found as a function of nonlinear integrated differential equations.

Physical problem and governing equation

Considering the flow of incompressible viscous nanoparticles in two dimensions across a porous stretching/shrinking surface. The surface is extended out within the direction of motion as taking on the x -axis, with the y -axis perpendicular to the slit. A uniform magnetic field B_0 is applied to the fluid flow. When two equal-strength forces are imposed towards the x -axis to restrain the liquid movement in the region $y > 0$. Suppose the sheet is submerged in a fluid with a consistent ambient temperature T_∞ as well as a surface temperature T_0 .

Considering that the fluid is inviscid, the principle of mass conservation is simplified³⁴ as follows:

$$\nabla \cdot \vec{q} = 0, \quad (1)$$

together with the principle of conservation of linear momentum defined as^{34,35} following

$$(\vec{q}_t + (\vec{q} \cdot \nabla) \vec{q}) = -\frac{\nabla p}{\rho_f} + \nu_{nf} \nabla^2 \vec{q} - \frac{\mu_{nf}}{\rho_{nf} K} \vec{q} - \frac{\sigma_{nf}}{\rho_{nf}} \vec{q}. \quad (2)$$

The modified system of equations for mass conservation and the sustained linear momentum^{34–36} are stated as

$$\frac{\partial u}{\partial x} + \frac{\partial v}{\partial y} = 0, \quad (3)$$

$$u \frac{\partial u}{\partial x} + v \frac{\partial u}{\partial y} = -\frac{1}{\rho_f} \frac{\partial p}{\partial x} + \frac{\mu_{nf}}{\rho_{nf}} \frac{\partial^2 u}{\partial y^2} - \frac{\mu_{nf}}{\rho_{nf} K} u - \frac{\sigma_{nf} B_0^2}{\rho_{nf}} u = 0, \quad (4)$$

and energy equation is

$$u \frac{\partial T}{\partial x} + v \frac{\partial T}{\partial y} = \chi \frac{\partial^2 T}{\partial y^2} - \frac{1}{(\rho C_p)_{nf}} \frac{\partial q_r}{\partial y}, \quad (5)$$

here (u, v) determines the velocities in the x and y axis correspondingly, dynamic viscosity of nanofluid is represented as μ_{nf} , ρ_{nf} is the nanofluids density, permeability of the fluid is denoted as K , σ_{nf} is the electrical conductivity of the nanofluid, $\chi = \frac{\kappa_{nf}}{(\rho C_p)_{nf}}$ is the thermal diffusivity of the nanofluid, whereas thermal conductivity of nanofluid is κ_{nf} , $(\rho C_p)_{nf}$ acts as heat capacitance of nanofluids.

The related boundary conditions^{3–5} are

$$\left. \begin{aligned} u(x, y) &= d\alpha x + \xi_1 \frac{\partial u}{\partial y} + \xi_2 \frac{\partial^2 u}{\partial y^2}, \quad v = v_c, \quad u(x, \infty) \rightarrow 0, \\ \theta(0) &= 0, \quad \theta(\infty) = 1 + \xi \theta'(0). \end{aligned} \right\}, \quad (6)$$

where corresponding slip coefficients of the first and second orders are represented through the quantities ξ_1 and ξ_2 . d is the stretching/shrinking parameter or proportionate shearing at the border. ξ is the temperature jump constant to be determined later. Moreover v_c determines mass transpiration factor, represents the suction or blowing depending on $v_c > 0$ or $v_c < 0$ respectively.

Implementing the following similarity conversation³⁷

$$u = \alpha x \frac{\partial f}{\partial \eta}, \quad v = -\sqrt{\alpha \nu_f} f(\eta), \quad \eta = \sqrt{\frac{\alpha}{\nu_f}} y, \tag{7}$$

$$\theta(\eta) = \frac{T - T_\infty}{T_w - T_\infty}.$$

here α is the constant. To model the movement of thermal radiation, the Rosseland approximation is utilized. In this approximate model, the heat flow is supposed to be proportional to the temperature differential, and it flows from solid surface to the liquid. As a result of this, the thermal radiation flux q_r to be expressed^{38–42} as follows

$$q_r = -\frac{4\sigma^*}{3k^*} \frac{\partial T^4}{\partial y}, \tag{8}$$

here σ^* stands for the Stefan-Boltzmann constant along with k^* stands for mean absorption coefficient. While T^4 may conceivably visualized as $T^4 \cong 4T_\infty^3 T - 3T_\infty^4$, and ensure there are suitable low temperature changes within the flowing fluid. With this, Eq. (8) can be written as

$$\frac{\partial q_r}{\partial y} = -\frac{16\sigma^* T_\infty^3}{3k^*} \frac{\partial^2 T}{\partial y^2}, \tag{9}$$

employing of similarity conversation in Eqs. (4)–(5), one obtain

$$\Gamma_1 \frac{\partial^3 f}{\partial \eta^3} + \Gamma_2 \left\{ f(\eta) \frac{\partial^2 f}{\partial \eta^2} - \left(\frac{\partial f}{\partial \eta} \right)^2 \right\} - \left\{ K_1 \Gamma_1 \frac{\partial f}{\partial \eta} + M \frac{\partial f}{\partial \eta} \right\} = 0, \tag{10}$$

$$\Gamma_3 (1 + N_r) \frac{\partial^2 \theta}{\partial \eta^2} + \text{Pr} \Gamma_4 f(\eta) \frac{\partial \theta}{\partial \eta} = 0, \tag{11}$$

here

$$\Gamma_1 = \frac{\mu_{nf}}{\mu_f}, \quad \Gamma_2 = \frac{\rho_{nf}}{\rho_f}, \quad \Gamma_3 = \frac{\kappa_{nf}}{\kappa_f} \text{ and } \Gamma_4 = \frac{(\rho C_p)_{nf}}{(\rho C_p)_f}.$$

$K_1 = \frac{\mu_f}{\rho_f \alpha K}$ is the inverse Darcy number (porosity parameter).

$M = \frac{\sigma_{nf} B_0^2}{\rho_f \alpha}$, acts as coefficient of Magnetic field (Hartmann number).

$\text{Pr} = \frac{\mu_f (C_p)_f}{k_f}$, be the Prandtl number.

In additionally,

$N_r = \frac{16\sigma^* T_\infty^3}{3k^* k_f}$ is the radiation parameter.

With transformed frontier constraints are

$$f(0) = V_c, \quad \left(\frac{\partial f}{\partial \eta} \right)_{\eta=0} = d + \lambda_1 \left(\frac{\partial^2 f}{\partial \eta^2} \right)_{\eta=0} + \lambda_2 \left(\frac{\partial^3 f}{\partial \eta^3} \right)_{\eta=0}, \quad \theta(\eta) = 1 + \xi \frac{\partial \theta}{\partial \eta}, \quad \text{at } \eta = 0, \tag{12}$$

$$\left(\frac{\partial f}{\partial \eta} \right)_{\eta \rightarrow \infty}, \quad \theta(\eta) \rightarrow 0, \quad \text{as } \eta \rightarrow \infty,$$

here $\lambda_1 = \xi_1 \sqrt{\frac{\alpha}{\nu_f}} > 0$, and $\lambda_2 = \xi_2 \frac{\alpha}{\nu_f} < 0$ are first and second order slips parameter, and mass transpiration factor is represented as $V_c = \frac{\nu_c}{\sqrt{\alpha \nu_f}}$.

The effective dynamic viscosity of the nanofluid is⁴³ stated as

$$\mu_{nf} = \frac{\mu_f}{(1 - \phi)^{2.5}}, \tag{13a}$$

nanofluid density is described⁴⁴ as

$$\rho_{nf} = \left\{ (1 - \phi) + \phi \left(\frac{\rho_s}{\rho_f} \right) \right\} \rho_f, \tag{13b}$$

the thermal conductivity of nanofluid is defined⁴⁵ as

$$\kappa_{nf} = \frac{\kappa_s + 2\kappa_f - 2\phi(\kappa_f - \kappa_s)}{\kappa_s + 2\kappa_f + \phi(\kappa_f - \kappa_s)}, \tag{13c}$$

effective heat capacitance of the nanofluids denoted⁴⁶ as

$$(\rho C_p)_{nf} = (1 - \phi)(\rho C_p)_f + \phi(\rho C_p)_s \quad (13d)$$

here ϕ is the volume fraction of the nanofluid.

Analytical solution for momentum equation

In the present article, we will show a closed form exact solution of Eq. (10) together with the boundary conditions (12), one may assume the solution has a format as

$$f(\eta) = A + B \exp(-\delta\eta), \quad (14)$$

where $\delta > 0$, is yet to be estimated latterly on, moreover the constants A and B must be calculated with employing Eq. (12).

presently,

$$A = V_c + \left(\frac{d}{\delta + \lambda_1 \delta^2 - \lambda_2 \delta^3} \right), \text{ with } B = \left(\frac{-d}{\delta + \lambda_1 \delta^2 - \lambda_2 \delta^3} \right), \quad (15)$$

In order obtained following algebraic equation by incorporating Eq. (13) into Eqs. (10):

$$\Gamma_1 \lambda_2 \delta^4 - (\Gamma_1 \lambda_1 + \Gamma_2 V_c \lambda_2) \delta^3 + (\Gamma_2 V_c \lambda_2 - \Gamma_1 - \Gamma_1 K_1 \lambda_2 - M \lambda_2) \delta^2 + (\Gamma_2 V_c + \Gamma_1 K_1 \lambda_1 + M \lambda_1) \delta + (\Gamma_2 d + \Gamma_1 K_1 + M) = 0, \quad (15a)$$

Equation (14) rewritten as

$$\delta^4 - p \delta^3 + q \delta^2 + r \delta + t = 0, \quad (16)$$

where

$$\left. \begin{aligned} p &= \frac{\Gamma_1 \lambda_1 + \Gamma_2 V_c \lambda_2}{\Gamma_1 \lambda_2}, \\ q &= \frac{\Gamma_2 V_c \lambda_2 - \Gamma_1 - \Gamma_1 K_1 \lambda_2 - M \lambda_2}{\Gamma_1 \lambda_2}, \\ r &= \frac{\Gamma_2 V_c + \Gamma_1 K_1 \lambda_1 + M \lambda_1}{\Gamma_1 \lambda_2}, \\ t &= \frac{\Gamma_2 d + \Gamma_1 K_1 + M}{\Gamma_1 \lambda_2}. \end{aligned} \right\} \quad (17)$$

Equation (15) gives four real roots which helps to provide solution for the current problem. Within this part we have to obtain an analytic approach to the momentum equation. Next move on to the analytical solution for the temperature equation which is discussed in further section.

Solution for the temperature region of fluid

Now introduce Eq. (13) in Eq. (11) we obtain as follow

$$\Gamma_3(1 + N_r) \frac{\partial^2 \theta}{\partial \eta^2} + \text{Pr} \Gamma_4 \{A + B \exp(-\delta\eta)\} \frac{\partial \theta}{\partial \eta} = 0, \quad (18)$$

In the following section, we use the Laplace transformation to examine the temperature solution in the context of the generalized incomplete gamma function and by framing a novel variable as

$t = e^{-\delta\eta}$, we achieve

$$(\Gamma_3 + N_r) t \frac{\partial^2 \theta}{\partial t^2} + (m - nt) \frac{\partial \theta}{\partial t} = 0, \quad (19)$$

where as

$$m = (\Gamma_3 + N_r) - \frac{\text{Pr} \Gamma_4 A}{\delta}, \quad n = \frac{\text{Pr} \Gamma_4 B}{\delta}. \quad (20)$$

with transformed boundary constraints are

$$\theta(0) = 0, \quad \theta(1) = 1 + \xi \left(\frac{\partial \theta}{\partial \eta} \right)_{\eta \rightarrow 1}. \quad (21)$$

Currently we interpolate Laplace transformation upon respective sides of the Eq. (18), once we achieve

$$s\{n - (\Gamma_3 + N_r)s\} \frac{\partial \Phi}{\partial s} + \{n + (m - 2(1 + N_r)s)\} \Phi(s) = 0, \quad (22)$$

here $\Phi(s)$ is the Laplace transformation of $\theta(t)$, that is $L\{\theta(t)\} = \Phi(s)$. To execute final expression, it should be observed that the initial modified boundary condition $\theta(0) = 0$ was used. So as to integrating the Eq. (20), we gathered

$$\Phi(s) = \frac{c}{s\left(s - \frac{n}{A_3+N_r}\right)^{1-\frac{m}{A_3+N_r}}}. \tag{23}$$

In which c is the integration constant which is to be determined later. For the sake of introduced the reverse Laplace transformation L^{-1} to Eq. (21). Thus, $\frac{m}{A_3+N_r}$ must be confined to be $\frac{m}{A_3+N_r} < 1$. As a result, we have follows

$$\theta(t) = cL^{-1}\left\{\frac{1}{s}\right\} * L^{-1}\left\{\frac{1}{\left(s - \frac{n}{A_3+N_r}\right)^{1-\frac{m}{A_3+N_r}}}\right\}, \tag{24}$$

$$\theta(t) = \frac{c}{\Gamma\left(1 - \frac{m}{A_3+N_r}\right)} \left(1 * e^{\frac{n}{A_3+N_r}t} t^{-\frac{m}{A_3+N_r}}\right), \tag{24a}$$

while $*$ signifies the convolution property as stated by

$$L^{-1}\{\Psi(s), \Theta(s)\} = \psi(t) * \varphi(t) = \int_0^t \psi(\mu)\varphi(t - \mu)d\mu, \tag{25}$$

In order that $L^{-1}\{\Psi(s)\} = \psi(t)$ with $L^{-1}\{\Theta(s)\} = \varphi(t)$. Consequently Eq. (22) develops as

$$\theta(t) = \frac{c}{\Gamma\left(1 - \frac{m}{A_3+N_r}\right)} \int_0^t \mu^{\frac{-m}{A_3+N_r}} e^{\frac{n\mu}{A_3+N_r}} d\mu, \tag{26}$$

Put $\sigma = -n\mu$ in Eq. (24), we obtain

$$\theta(t) = \frac{c}{\Gamma\left(1 - \frac{m}{A_3+N_r}\right)} \left(\frac{-1}{n}\right)^{1-\frac{m}{A_3+N_r}} \Gamma\left(1 - \frac{m}{A_3+N_r}, 0, \frac{-n}{A_3+N_r}t\right), \tag{27}$$

now accomplish second modified boundary constraints i.e. $\theta(1) = 1 + \xi\left(\frac{\partial\theta}{\partial\eta}\right)_{\eta \rightarrow 1}$, we acquire the value of c as

$$c = \frac{\Gamma\left(1 - \frac{m}{A_3+N_r}\right)}{\left(\frac{-1}{n}\right)^{1-\frac{m}{A_3+N_r}} \Gamma\left(1 - \frac{m}{A_3+N_r}, 0, \frac{-n}{A_3+N_r}\right) - \xi e^{\frac{n}{A_3+N_r}}}, \tag{28}$$

currently substitute Eq. (26) into Eq. (25), hence, $\theta(t)$ is presented in the precise form shown below

$$\theta(t) = \frac{\Gamma\left(1 - \frac{m}{A_3+N_r}, 0, -\frac{n}{A_3+N_r}e^{-\beta\eta}\right)}{\Gamma\left(1 - \frac{m}{A_3+N_r}, 0, -\frac{n}{A_3+N_r}\right) - \xi(-n)^{1-\frac{m}{A_3+N_r}} e^{\frac{n}{A_3+N_r}}}, \tag{29}$$

in this section we obtained exact analytic solution for energy equation in terms of generalized gamma functions with employing Laplace transformation formula. Proceed to following section, where we must discuss the current problem outcomes.

Interpretation of results

We go into greater detail about the physical aspects of the interest constraints related to the current blood flow models. Setting the numerical value of the Prandtl number Pr is 21 for blood. The range of the parameter taken as $0.5 \leq M \leq 5, 0.1 \leq \phi \leq 0.6, -1 \leq V_c \leq 4, 0.1 \leq K_1 \leq 5, 0.2 \leq \lambda_1 \leq 6, -6 \leq \lambda_2 \leq 0.5, 0.1 \leq \xi \leq 5$, and $0.01 \leq N_r \leq 5$. The results found to be in good agreement. To analyze the flow and heat transfer characteristics of the nanofluid. The computed analytical results of the velocity, temperature as well as shear stress, rates of heat transfer for a benefits of the regulating circumstances, particularly magnetic field (M), stretching/shrinking strength factor (d), first (λ_1) together with second order (λ_2) Navier slip conditions, mass transpiration parameter (V_c), inverse Darcy number parameter (K_1), Prandtl number (Pr) together with radiation parameter (N_r) are demonstrated graphically. Also the physical properties of nanofluids in base fluid are mentioned in the Table 1. Validation of present study and already existing works as shown in Table 2.

The physical mechanism of the problem is given in the Fig. 1. The stimulus of magnetic parameter M on velocity as well as temperature profile is demonstrated through a Fig. 2a–c, which illustrates the role of hartmann number upon velocity outline $f(\eta)$, $\frac{\partial f}{\partial \eta}$, with thermal distribution $\theta(\eta)$. Figure 2a,b It is observed that rising strength of hartmann number diminishes momentum of the fluid. Hence magnetic field generates force which

Sl. No.	Nanofluid/base fluid	ρ (kg/m ³)	κ (W/mK)	C_p (J/kg K)
1.	Blood	1053	0.492	3594
2.	Silver	10,500	429	235
3.	Copper	8933	401	385

Table 1. Thermo-physical properties of nanofluid^{35,47–50}.

Related works by other authors	Fluids	Value of δ
Mahabaleshwar ³⁴	Non-Newtonian	$f(\eta) = A_1 + B_1 \exp(-\delta\eta)$ Where $A_1 = V_c + \frac{d}{\delta + \Gamma_1 \delta^2 - \Gamma_2 \delta^3}$, $B_1 = -\frac{d}{\delta + \Gamma_1 \delta^2 - \Gamma_2 \delta^3}$.
Fang ⁵¹	Non-Newtonian	$f(\eta) = a + b \exp(-\beta\eta)$ Where $a = s + \frac{1}{\beta + \Gamma \beta^2 - \delta \beta^3}$, $b = -\frac{1}{\beta + \Gamma \beta^2 - \delta \beta^3}$. Pr Present Present work Non-Newtonian Pp Prese
Present work	Non-Newtonian	$f(\eta) = A + B \exp(-\delta\eta)$ Where $A = V_c + \frac{d}{\delta + \lambda_1 \delta^2 - \lambda_2 \delta^3}$, $B = -\frac{d}{\delta + \lambda_1 \delta^2 - \lambda_2 \delta^3}$

Table 2. Comparison of the current research and relevant studies by other authors.

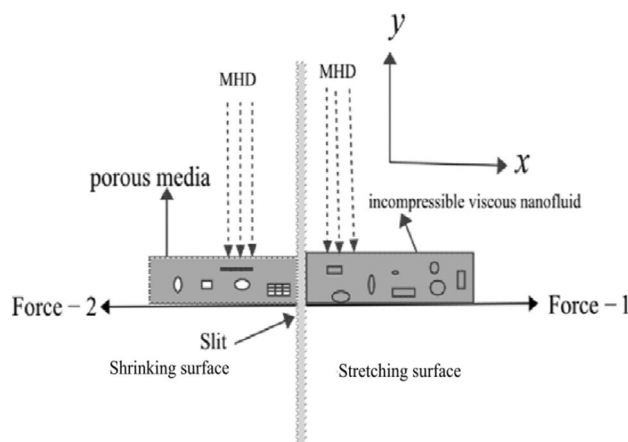


Figure 1. Physical mechanism of the flow problem.

acts reverse direction. The flow field encounters resistance from this force (Lorentz force) and rate of transport is minimized considerably by keeping the values at $d = 1$, $\lambda_1 = 0.5$, $\lambda_2 = 0.05$, and $K_1 = 0.1$. The mobility of the nanoparticles inside the surface is reduced by increasing the intensity of the hartmann number, which also has an adverse effect on the bloods viscosity. Also we noticed that copper-blood nanofluid has more velocity distribution as compared with silver-blood nanofluid. Figure 2c depicts the changes of the nanofluid hartmann number on temperature distribution. It has been noted that as hartmann number broadening, the temperature also growing. Due to nanoparticles, bulk temperature as well as thermal boundary layer develops in the nanoparticles because of its more heat conductance. Besides silver nanoparticles has more temperature than that of copper nanoparticles, in view of the fact that silver has a higher heat conductance than copper nanoparticles.

Figure 3a,b presents the tangential velocity distribution for several desirability of the primary order slip λ_1 parameter with keeping the values at $d = -1$, $M = 0.5$, $\lambda_2 = 0.1$, $K_1 = 0.5$, and $V_c = 2$. This graph apparently express that the lowering the Navier slip, upshots in the diminishes the velocity barrier. Here perceives that width of the nanofluid velocity boundary subject to upper solution branch is reduced as correlated to the lower solution branch. Likewise, one can observe the relationship between the growing velocity boundary width and improvements in the stretching/shrinking factor under stated slip parameter with mass suction parameter. Consequently, decline in mass suction causes a reduction in the acceleration border for other static physical parameters. Although when mass injection is included, the mobility barrier grows as the slip parameter's values rise. As a result, the slip parameter has a big impact on the flow structure and indeed the rate of change in mobility boundary layer width.

The impact of the velocity slip parameters λ_1 and λ_2 on the velocity profile is displayed in the Fig. 4a–c for the silver and copper nanofluids respectively. With rising values of slip parameters, a decline in the dimensionless velocity field is shown in the Fig. 4a–c. when the nanofluids speed lowers and also the velocity slip parameter

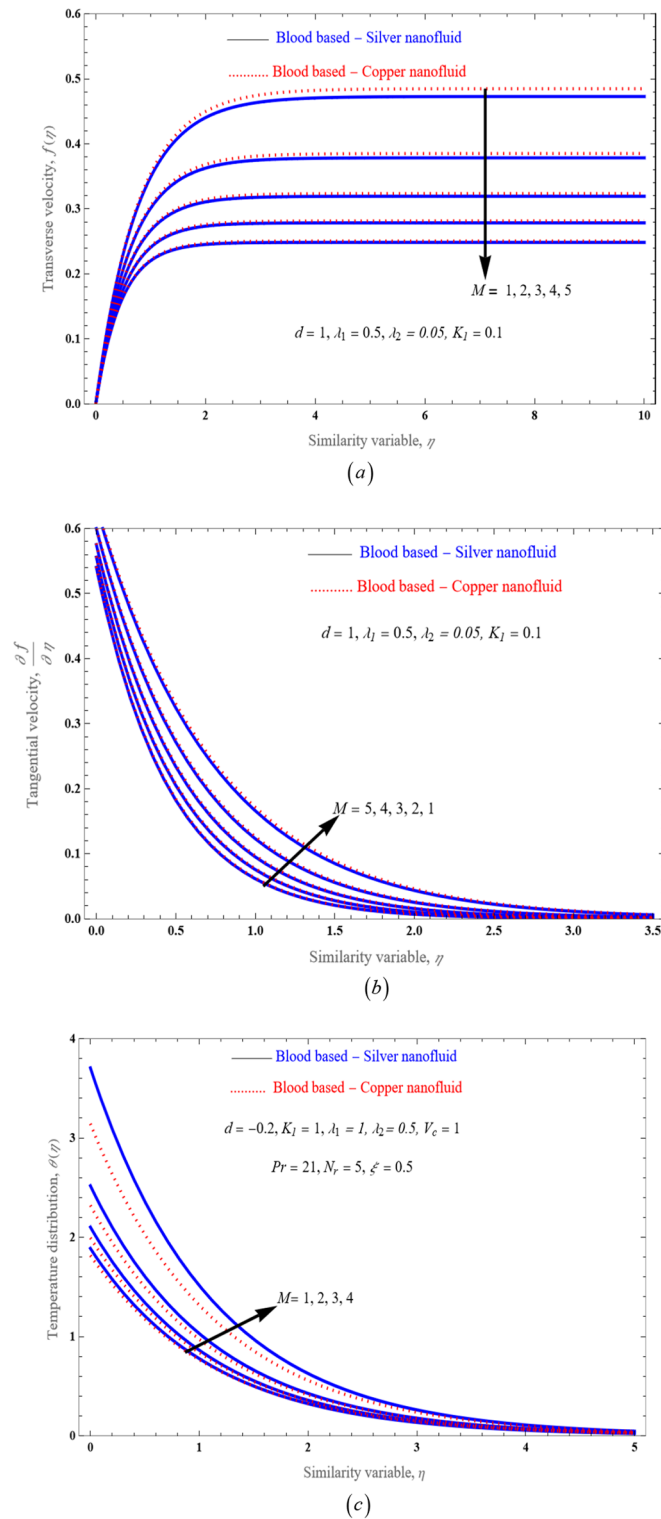


Figure 2. An impact of magnetic field M on velocity distribution (a,b) and temperature distribution (c).

improves. This is due to truly under slip effects, the movement of the stretched surface is different from the speed of the nanofluid flow nearer to the surface.

Figure 5a be drawn to concluded that influence of mass suction/injection factor V_c upon velocity distribution. It is observed that movement of nanofluid flow is decreases (velocity profile reduces) with uplifting value of the suction/injection parameter. Whereas from Fig. 5b it is noticed that acceleration of fluid flow improved as enhancing the quantity of V_c value.

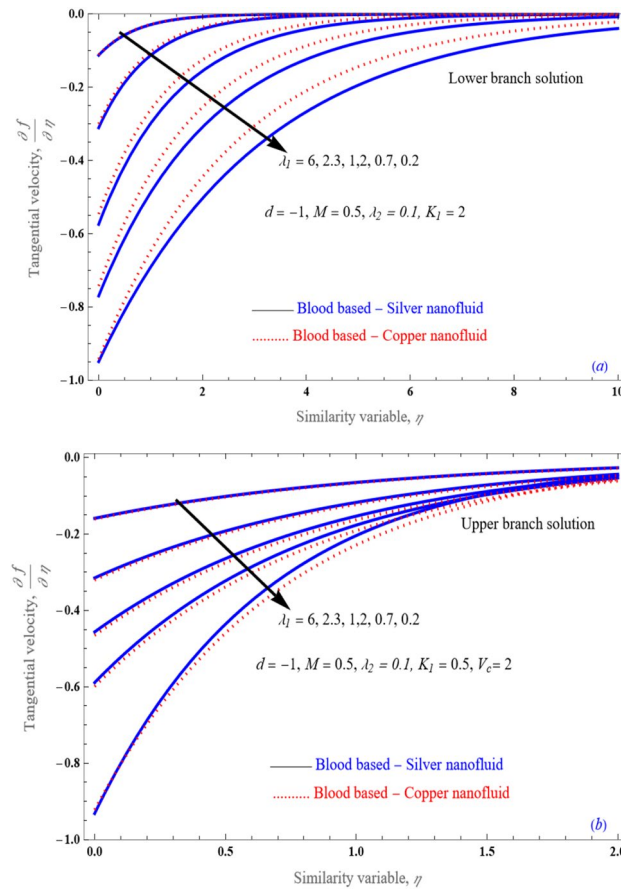


Figure 3. An impact of first order Navier slip λ_1 on (a) transverse velocity and (b) tangential velocity profile.

Figure 6 illustrates deviations in the temperature field with various values of ξ respectively, while sustaining all other variables at the specified levels. Plot demonstrating that as climbs in the stretching sheet, the temperature velocity does as well. It results in the prediction that the boundary layer will expand as various values improve. It is clearly shows The energy layers increases with an increase in thermal jump.

The slip effect parameter upon temperature is represented in Fig. 7. In the presence of a magnetic field and a thermal jump, the fluid is flowing more freely and consistently as λ_1 raises. Consequently, the profile is more consistent, as well as the heat transmission rate is reduced.

Figure 8 illustrates the change in temperature profiles induced by an increment in the value of a porosity component. A boost in the value of the porosity component results in a lowering impact on the temperature distribution. The thickness of the thermal boundary layer becomes thinner with the increase of the porosity parameter. Figure 9 explores how the temperature enhances while thermal radiation accumulates. Although radiation has the consequence of grows the rate at which a fluid's temperature is raised and consequently improving that temperature, the conclusion is subjectively consistent with the assumptions. Since higher radiation parameter values merely raise the surface heat transfer, rendering the fluid hotter.

An effect of solid volume fraction of the nanofluid on temperature distribution is portrayed in Fig. 10. The nanoparticles volume fraction has improved. since temperature conductance rises among increasing nanoparticle volume values. Physically, this tendency is in line with the premise that copper solid particles have a thermal conductivity that is larger than the silver nanofluids thermal conductivity. The optimal space for δ against V_c as various Porosity K_1 values is shown in Fig. 11a–c. Expression (15a) is really reduced to a cubic equation by assuming $\lambda_2 = 0$, and with the right selection of λ_1 , and K_1 . From Fig. 11a–c, we observed that the flow solution domain is varied because of nature of the porosity value. An effects λ_1 besides porosity parameter K_1 upon solution space δ relative mass suction/injection V_c is displayed in Fig. 12a–c. The dispersion curve is forced towards the slit by the appearance of a higher slip. The movement of a viscous liquid in a porous material with slip at a stretched border is very distinct beyond that of a shrinking border.

Figure 13 demonstrated the upshots of several physical characteristics on the shear stress spectrum. In such graph, the overall impacts on the porous solid can be seen at overlap locations for the shear stress spectra. At the wall's boundary, shear increases as the values of λ_1 , λ_2 and porosity parameter rise.

Figure 14a–d demonstrate performance of the solution space δ of against mass suction/injection parameter V_c for varying values of λ_1 with fixed the value at $M = 1$, $\lambda_2 = 0.01$ and 0.5. This figures shows the flow patterns of the fluid in the specified region. In fact, by choosing $\lambda_2 = 0$, and $M = 0$, Eq. (15a) reduces to a cubic equation and with the proper choice of λ_1 , Γ_1 , Γ_2 , and K_1 , and the results are reduced to those obtained by^{28,51,52}.

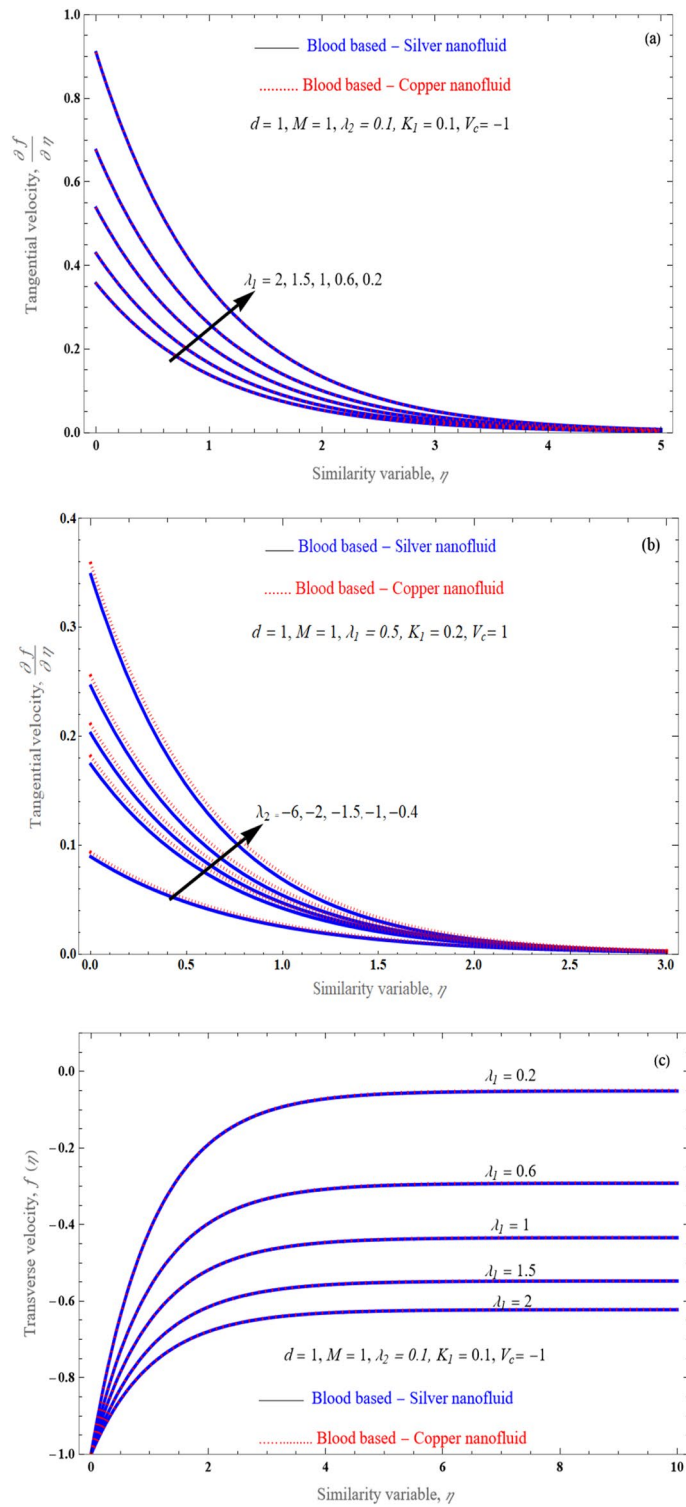


Figure 4. An impact of slip parameter λ_1 and λ_2 on velocity profile for stretching surface.

Concluding remarks

In present study we conduct the theoretical study on laminar stream of viscous incompressible liquid through a penetrable stretching/shrinking sheet under the influence of thermal radiation as well as magnetohydrodynamic effects. Also carry through Navier slip conditions along with mass suction/injection parameter is considered. A similarity conversion is employed to convert the controlling PDEs for momentum and temperature to ODEs.

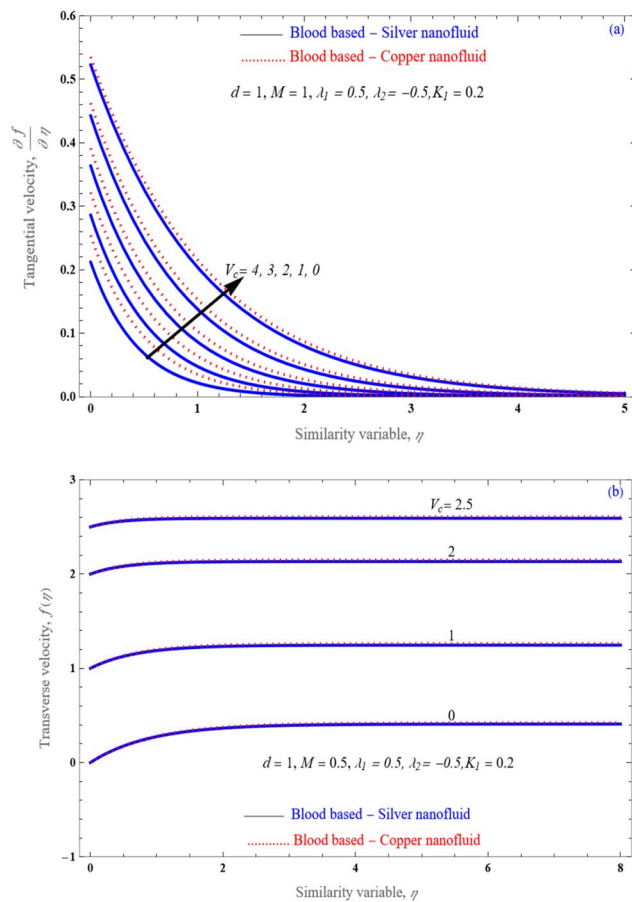


Figure 5. An impact of V_c on (a) velocity profile and (b) tangential velocity profile for stretching case.

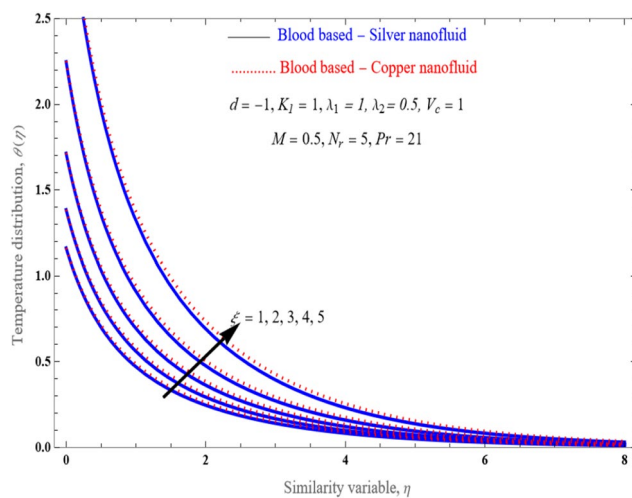


Figure 6. An impact of ξ on temperature profile $\theta(\eta)$.

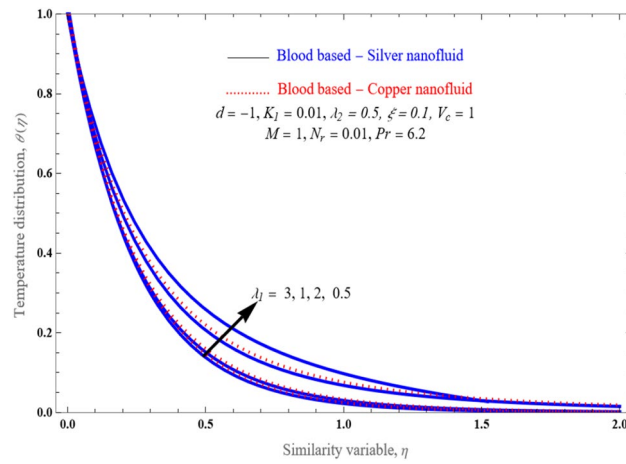


Figure 7. An impact of first order slip factor λ_1 on temperature profile $\theta(\eta)$.

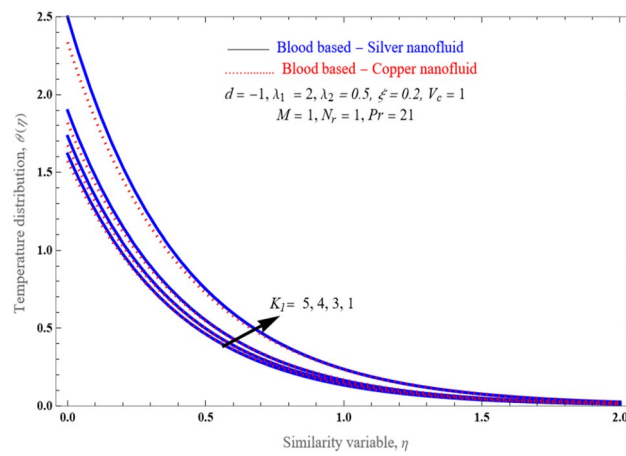


Figure 8. An impact of inverse Darcy number (porosity) on temperature distribution $\theta(\eta)$.

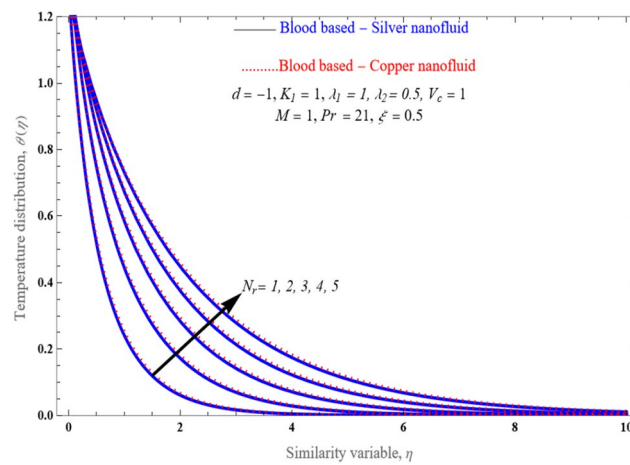


Figure 9. An impact of N_r on temperature distribution $\theta(\eta)$.

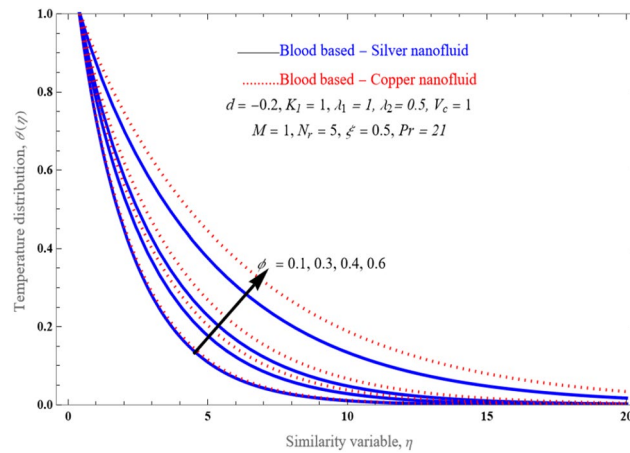


Figure 10. An impact of various values of solid volume fraction ϕ on temperature profile.

These equations are solved analytically. Ag-blood and Cu-blood nanofluids are taken into consideration in the study. Plots are employed to examining an impacts of various temperature as well as velocity pattern properties. The comprehensive list of the study's outputs are:

- As the magnetic parameter M increases, the velocity profile and the width of the border layer of momentum decline and also noticed that copper-blood nanofluid have more velocity compared to that of silver-blood nanofluid.
- Silver nanoparticles have a higher temperature than copper nanoparticles have been observed.
- With an increment in the velocity slip parameter, the velocity profile reduces while the temperature profile climbs.
- The Prandtl number has the result of diminishing the width of the thermal boundary layer.
- The temperature of the nanoparticles also rises as the radiation parameter R grows.
- The rate of heat is minimized by the velocity slip parameter.

Several preceding studies serve as the current study limiting points:

lim

- $M \rightarrow 0, q_r \rightarrow 0$, {our results \rightarrow Mahabaleshwar et al.³⁴}
- $T \rightarrow 0$
- By setting $\lambda_2 = 0$, Eq. (15a) reduces to results of Fang et al.⁵¹, Zhang et al.⁵² and Yao et al.⁵³.

Further extensions of the current work can be implemented incorporating new physical mechanisms, such as Newtonian or non-Newtonian fluid rheology.

Validation

The research reveals the effect of Navier's slip and MHD on laminar boundary layer flow and heat transfer for an incompressible non-Newtonian nanofluid over a porous stretching/shrinking sheet with mass transpiration. In the absences of magnetic field $M = 0$, and solid volume fraction $\phi = 0$ leads to the results of Mahabaleshwar et al.³⁴. In the absences of magnetic field $M = 0$, $Da^{-1} = 0$, and $\phi = 0$ with absences of temperature leads to the results of Fang et al.⁵¹.

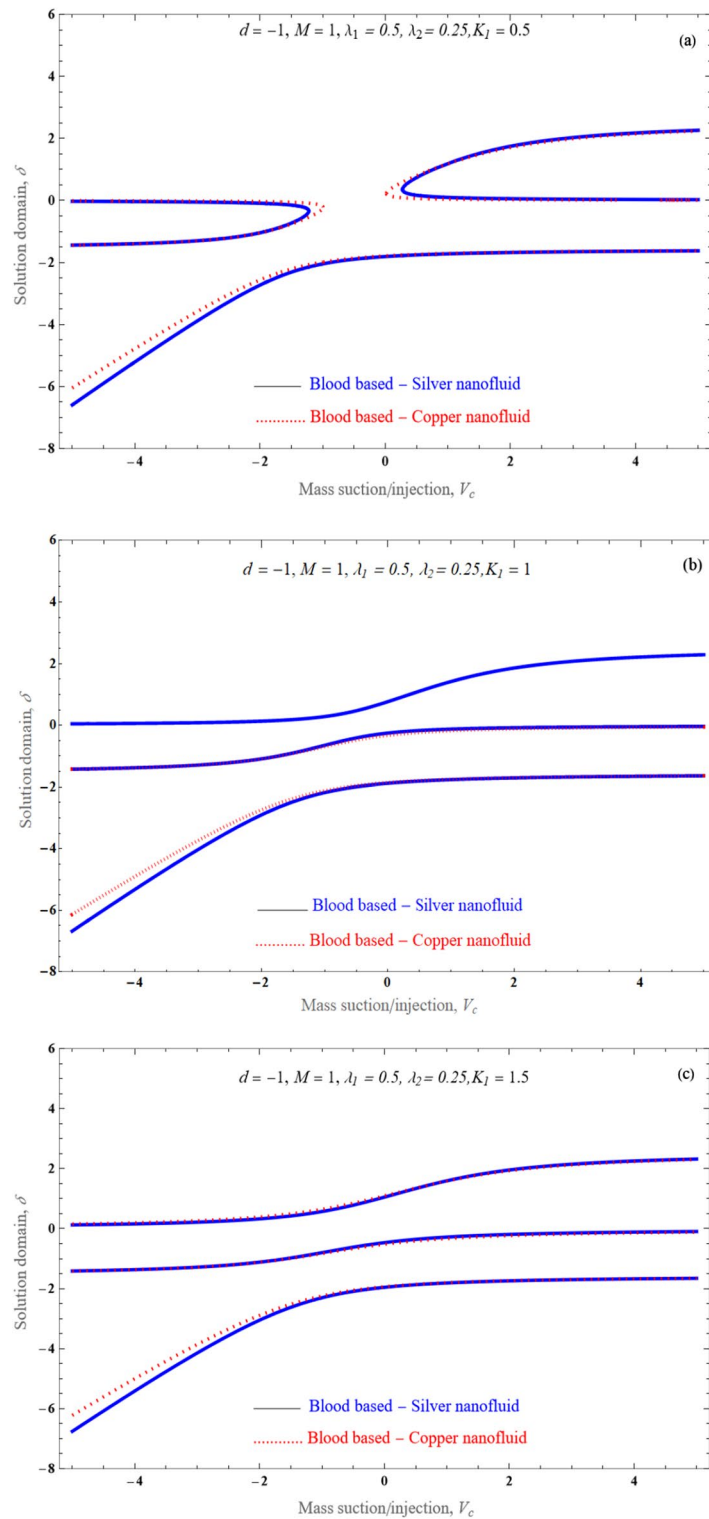


Figure 11. (a–c) Existence of domain δ against parameter V_c for several values of K_1 .

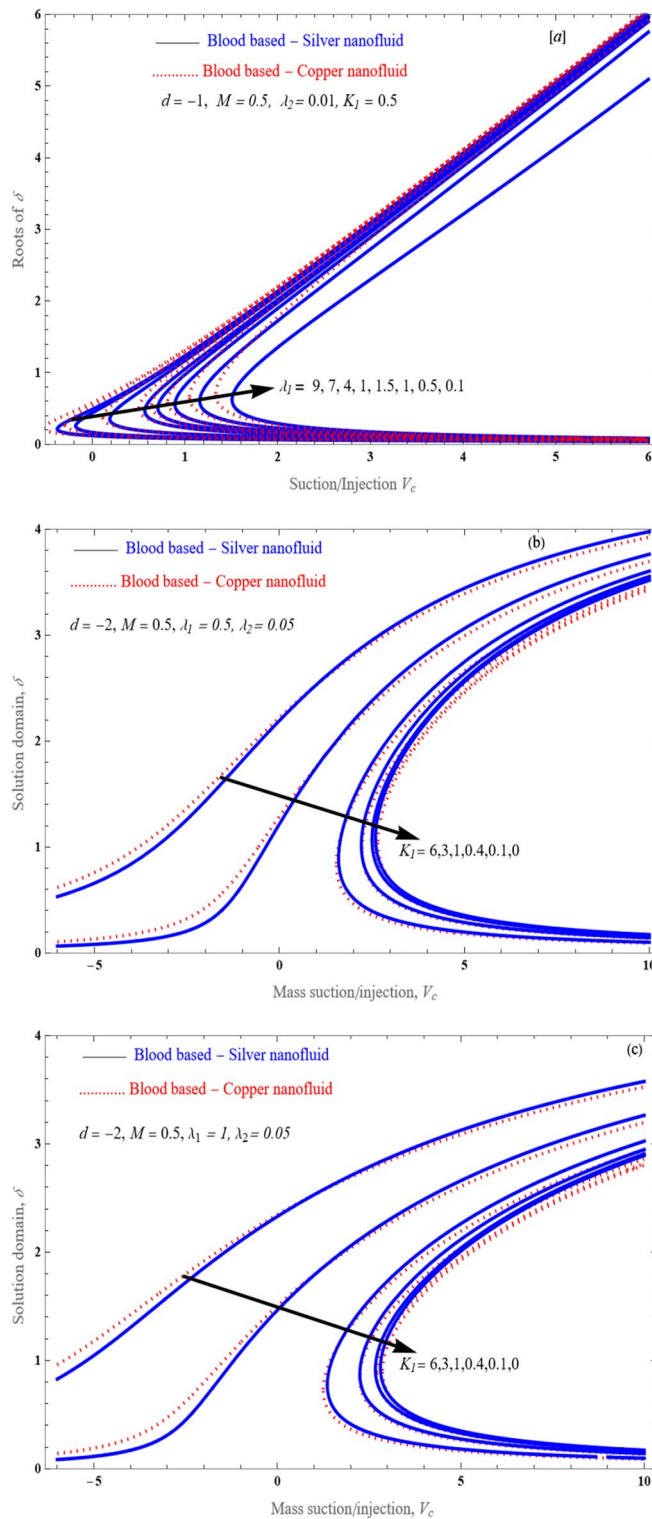


Figure 12. An impact of λ_1 (a) and K_1 (b,c) on solution domain of δ is plotted against the Mass suction/injection parameter.

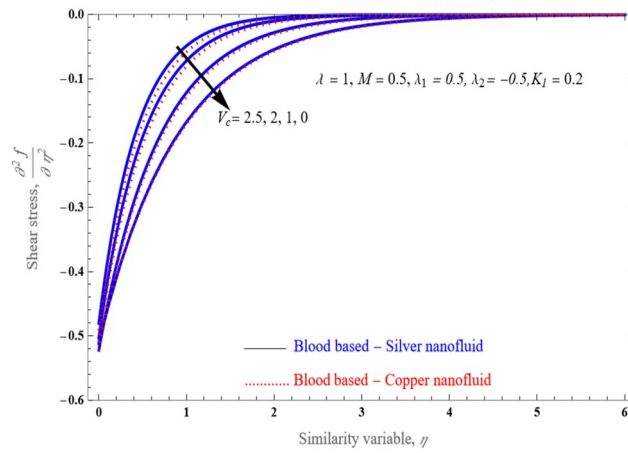


Figure 13. An impact of various values of V_c on the shear stress profile for stretched condition and other parameter are fixed.

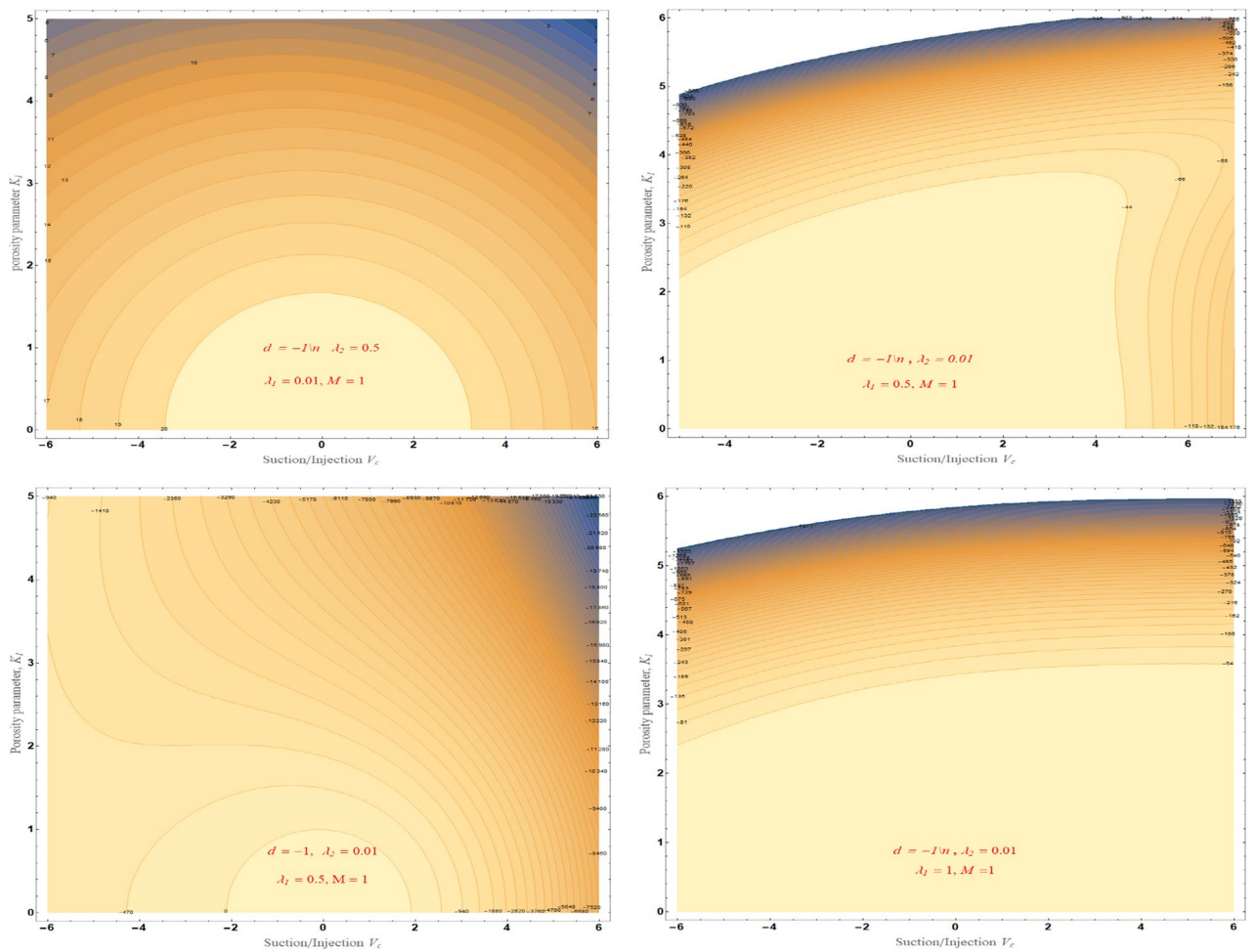


Figure 14. The solution region of porosity parameter K_1 against mass suction/injection parameter V_c for stretched case.

Data availability

Data that support the findings of this study are available from the corresponding author upon reasonable request.

Code availability

Codes that support the findings of this study are available from the corresponding author upon reasonable request.

Received: 7 April 2023; Accepted: 20 July 2023

Published online: 03 August 2023

References

- Choi, S. U. S. & Eastman, J. A. Enhancing thermal conductivity of fluids with nanoparticles. *ASME Publ. Fed.* **231**, 99–105 (1995).
- Eastman, J. A., Choi, S. U. S., Li, S., Yu, W. & Thompson, L. J. Anomalous increased effective thermal conductivities of ethylene glycol-based nanofluids containing copper nanoparticles. *Appl. Phys. Lett.* **78**, 718–720 (2001).
- Pozhar, L. A., Kontar, E. P. & Hua, M. Z. C. Transport properties of nanosystems: Viscosity of nanofluids confined in slit nanopores. *J. Nanosci. Nanotechnol.* **2**, 209–227 (2002).
- Pozhar, L. A. & Gubbins, K. E. Quasi hydrodynamics of nanofluids mixtures. *Phys. Rev. E* **56**, 5367–5396 (1997).
- Pozhar, L. A. Structure and dynamics of nanofluids: Theory and simulations to calculate viscosity. *Phys. Rev. E* **61**, 1432–1446 (2000).
- Rashidi, M. M., Ghahremanian, S., Toghraie, D. & Roy, P. Effect of solid surface structure on the condensation flow of argon in rough nanochannels with different roughness geometries using molecular dynamics simulation. *Int. Commun. Heat Mass Transf.* **117**, 104741 (2020).
- Mansoury, D., Doshmanziari, F. I., Rezaie, S. & Rashidi, M. M. Effect of Al_2O_3 /water nanofluid on performance of parallel flow heat exchangers. *J. Therm. Anal. Calorim.* **135**, 625–643 (2019).
- Rashad, A. M., Rashidi, M. M., Lorenzini, G., Ahmed, S. E. & Aly, A. M. magnetic field and internal heat generation effect on the free convection in a rectangular cavity filled with a porous medium saturated with *Cu*-water nanofluids. *Int. J. Heat Mass Transf.* **104**, 878–889 (2017).
- Hatami, M., Zhou, J., Geng, J., Song, D. & Jing, D. Optimization of a lid-driven T-shaped porous cavity to improve the nanofluids mixed convection heat transfer. *J. Mol. Liq.* **231**, 620–631 (2017).
- Sheikholeslami, M. New computational approach for exergy and entropy analysis of nanofluids under the impact of Lorentz force through a porous media. *Comput. Methods Appl. Mech. Eng.* **344**, 319–333 (2019).
- Hatami, M. & Jing, D. Optimization of wavy direct absorber solar collector (WDASC) using Al_2O_3 -water nanofluid and RSM analysis. *Appl. Therm. Eng.* **121**, 1040–1050 (2017).
- Tang, W., Hatami, M., Zhou, J. & Jing, D. Natural convection heat transfers in a nanofluid-filled cavity with double sinusoidal wavy walls of various phase deviations. *Int. J. Heat Mass Transf.* **115**, 430–440 (2017).
- Hatami, M. Nanoparticles migration around the heated cylinder during the RSM optimization of a wavy-wall enclosure. *Adv. Powder Technol.* **28**, 890–899 (2017).
- Alves, H. Existence of electromagnetic. *Nature* **150**, 405–406 (1942).
- Mahabaleswar, U. S., Aly, E. H. & Vishalakshi, A. B. MHD and thermal radiation flow of graphene casson nanofluid stretching/shrinking sheet. *Int. J. Appl. Comput. Math.* **8**, 1–48 (2022).
- Mahabaleswar, U. S., Vishalakshi, A. B. & Anderson, H. I. Hybrid nanofluid flow past a stretching/shrinking sheet with thermal radiation and mass transpiration. *Chin. J. Phys.* **75**, 152–168 (2022).
- Sneha, K. N., Mahabaleswar, U. S., Bennacer, R. & Ganaoui, M. E. L. Darcy brinkman equation for hybrid dusty nanofluid with heat transfer and mass transpiration. *Computation* **9**, 118 (2021).
- Anusha, T., Mahabaleswar, U. S. & Sheikhejad, Y. An MHD of nanofluid over a porous stretching/shrinking plate with mass transpiration and Brinkmann ratio. *Transp. Porous. Media* **142**, 333–352 (2022).
- Mahabaleswar, U. S., Anusha, T. & Hatami, M. The MHD Newtonian hybrid nanofluid flow and mass transfer analysis due to super linear-stretching sheet embedded in porous medium. *Sci. Rep.* **11**, 1–17 (2021).
- Sneha, K. N., Mahabaleswar, U. S., Chan, A., Hatami, M. Investigation of radiation and MHD on non-Newtonian fluid flow over a stretching/shrinking sheet with CNTs and mass transpiration. In *Waves Random Complex Media*. 1–20 (2022).
- Chahregh, H. S. & Dinarvand, S. TiO_2 -Ag/blood hybrid nanofluid flow through an artery with applications of drug delivery and blood circulation in the respiratory system. *Int. J. Numer. Methods Heat Fluid Flow* **30**, 4775–4796 (2020).
- Misra, J. C. & Chandra, S. Effect of couple stresses on electro kinetic oscillatory flow of blood in the microcirculatory system. *J. Mech. Med. Biol.* **18**, 1850035 (2018).
- Ghassemi, M., Shahidian, A., Ahmadi, G. & Hamian, S. A new effective thermal conductivity model for a bio-nanofluid (blood with nanoparticles Al_2O_3). *Int. Comm. Heat Mass Transf.* **37**, 929–934 (2010).
- Shankar, D. S. & Lee, U. Mathematical modelling of pulsatile flow of non-Newtonian fluid in stenosed arteries. *Commun. Nonlinear Sci. Numer. Simul.* **14**, 2971–2981 (2019).
- Nadeem, S. & Akbar, N. S. Influence of heat and chemical reactions on Walter's B fluid model for blood flow through a tapered artery. *J. Taiwan Inst. Chem. Eng.* **42**, 67–75 (2011).
- Shahzadi, I. & Nadeem, S. inclined magnetic field analysis for metallic nanoparticles submerged in blood with convective boundary condition. *J. Mol. Liq.* **230**, 61–73 (2017).
- Ijaz, S. & Nadeem, S. Consequence of blood medicated nano transportation as drug agent to attenuate the atherosclerotic lesions with permeability impacts. *J. Mol. Liq.* **262**, 565–575 (2018).
- Rehman, K. U., Malik, M. Y., Zehra, I. & Alqarni, M. S. Group theoretical analysis for MHD flow fields: A numerical result. *J. Braz. Soc. Mech. Sci. Eng.* **41**, 156 (2019).
- Bilal, S. *et al.* Numerical investigation on D viscoelastic fluid due to exponentially stretching surface with magnetic effects: An application of non-Fourier flux theory. *Neural Comput. Appl.* **30**, 2749–2758 (2018).
- Rehman, K. U., Malik, M. Y., Makinde, O. D. & Malik, A. A. A comparative study of nanofluids flow yields by an inclined cylindrical surface in a double stratified medium. *Eur. Phys. J. Plus.* **132**, 427 (2017).
- Ali, U., Alqahtani, A. S., Rehman, K. U. & Malik, M. Y. On Cattaneo-Christov heat flux analysis with magnetohydrodynamic and heat generation effects in a Carreau nanofluid over a stretching sheet. *Rev. Mex. Fis.* **65**, 479–488 (2019).
- Rehman, K. U., Alshomrani, A. A. & Malik, M. Y. Carreau fluid flow in a thermally stratified medium with heat generation/absorption effects. *Case Stud. Therm. Eng.* **12**, 16–25 (2018).
- Rehman, K. U., Khan, A. A., Malik, M. Y., Ali, U. & Naseer, M. Numerical analysis subjected to double stratification and chemically reactive species on williamson dual convection fluid flow yield by an inclined stretching cylindrical surface. *Chin. J. Phys.* **55**, 1637–1652 (2017).

34. Mahabaleshwar, U. S., Kumar, P. N. V., Nagaraju, K. R., Bognár, G. & Nayakar, S. N. R. A new exact solution for the flow of a fluid through porous media for a variety of boundary conditions. *Fluids*. **4**, 125 (2019).
35. Rajagopal, K. R. On a hierarchy of approximate models for flows of incompressible fluids through porous solids. *Math. Model. Methods Appl. Sci.* **17**, 215–252 (2007).
36. Mahabaleshwar, U. S., Maranna, T. & Sofos, F. Analytical investigation of an incompressible viscous laminar Casson fluid flow past a stretching/shrinking sheet. *Sci. Rep.* **12**, 18404 (2022).
37. Eldabe, N. & Zeid, M. A. Thermal diffusion and diffusion thermo effects on the viscous fluid flow with heat and mass transfer through porous medium over a shrinking sheet. *J. Appl. Math.* **1**, 584534 (2013).
38. Vishalakshi, A. B., Maranna, T., Mahabaleshwar, U. S. & Laroze, D. An effect of MHD on non-Newtonian fluid flow over a porous stretching/shrinking sheet. *Appl. Sci.* **12**, 4937 (2022).
39. Maranna, T., Sneha, K. N., Mahabaleshwar, U. S., Sarris, I. E. & Karakasidis, T. E. An effect of radiation and MHD Newtonian fluid over a stretching/shrinking sheet with CNTs and mass transpiration. *Appl. Sci.* **12**, 5466 (2022).
40. Zhu, J., Liu, Y. & Cao, J. Effect of second-order velocity slip and the different spherical nanoparticles on nanofluid flow. *Symmetry*. **13**, 64 (2021).
41. Maranna, T., Mahabaleshwar, U. S., Perez, L. M. & Manca, O. Flow of viscoelastic ternary nanofluid over a shrinking porous medium with heat source/sink and radiation. *Therm. Sci. Eng. Prog.* **40**, 101791 (2023).
42. Mahabaleshwar, U. S., Maranna, T., Perez, L. M. & Ravichandra Nayakar, S. N. An effect of magnetohydrodynamic and radiation on axisymmetric flow of non-Newtonian fluid past a porous shrinking/stretching surface. *J. Magn. Magn. Mater.* **571**, 170538 (2023).
43. Hassain, S. T., Nadeem, S. & Ul Haq, R. Model based analysis of micropolar nanofluid flow over a stretching surface. *Eur. Phys. J. Plus.* **129**, 1–10 (2014).
44. Chamkha, A. J. & Aly, A. M. MHD free convection flow of a nanofluid past a vertical plate in the presence of heat generation or absorption effects. *Chem. Eng. Commun.* **198**, 425–441 (2010).
45. Mahdy, A. Unsteady mixed convection boundary layer flow and heat transfer of nanofluid due to stretching sheet. *Nuclear. Eng. Des.* **249**, 248–255 (2012).
46. Benos, L. T., Polychronopoulos, N. D., Mahabaleshwar, U. S., Lorenzini, G. & Sarris, I. E. Thermal and flow investigation of MHD natural convection in a nanofluid-saturated porous enclosure: an asymptotic analysis. *J. Therm. Anal. Calorim.* **143**, 751–765 (2021).
47. Mahabaleshwar, U. S., Kumar, P. N. V. & Shermet, M. Magnetohydrodynamics flow of a nanofluid driven by a stretching/shrinking sheet with suction. *Springer Plus.* **5**, 1–9 (2016).
48. Siddiqui, A. & Shankar, B. Thermal radiation and slip effects on MHD flow and heat transfer of a Casson nanofluid over a stretching sheet. *J. Nanofluids.* **7**, 100–107 (2018).
49. Hayat, T., Kiran, A., Imtiaz, M. & Alsaedi, A. Hydromagnetic mixed convection flow of copper and silver water nanofluid due to curved stretching sheet. *Results Phys.* **6**, 904–910 (2016).
50. Shahzad, F. et al. MHD pulsatile flow of blood-based silver and gold nanoparticles between two concentric cylinders. *Symmetry*. **14**, 2254 (2022).
51. Fang, T. & Aziz, A. Viscous flow with second order slip velocity over a stretching sheet. *Zeitschrift Fur Naturforschung A.* **65**, 195–203 (2010).
52. Fang, T. G., Zhang, J. & Yao, S. S. Slip magnetohydrodynamic viscous flow over a permeable shrinking sheet. *Chin. Phys. Lett.* **27**, 124702 (2010).
53. Fang, T., Yao, S., Zhang, J. & Aziz, A. Viscous flow over a shrinking sheet with a second order slip flow model. *Commun. Nonlinear Sci. Numer. Simul.* **15**, 1831–1842 (2010).

Author contributions

Conceptualization, U.S.M.; methodology, T.M.; validation, T.M. and S.M.S.; formal analysis, U.S.M.; investigation, T.M.; data curation, writing—original draft preparation, U.S.M. and M.H.; writing—review and editing, M.H.; visualization, T.M. and S.M.S.; supervision, U.S.M. and M.H. All authors have read and agreed to the published version of the manuscript.

Competing interests

The authors declare no competing interests.

Additional information

Correspondence and requests for materials should be addressed to U.S.M. or M.H.

Reprints and permissions information is available at www.nature.com/reprints.

Publisher's note Springer Nature remains neutral with regard to jurisdictional claims in published maps and institutional affiliations.



Open Access This article is licensed under a Creative Commons Attribution 4.0 International License, which permits use, sharing, adaptation, distribution and reproduction in any medium or format, as long as you give appropriate credit to the original author(s) and the source, provide a link to the Creative Commons licence, and indicate if changes were made. The images or other third party material in this article are included in the article's Creative Commons licence, unless indicated otherwise in a credit line to the material. If material is not included in the article's Creative Commons licence and your intended use is not permitted by statutory regulation or exceeds the permitted use, you will need to obtain permission directly from the copyright holder. To view a copy of this licence, visit <http://creativecommons.org/licenses/by/4.0/>.

© The Author(s) 2023